ACS OMEGA

http://pubs.acs.org/journal/acsodf

Article

CISS-Based Label-Free Novel Electrochemical Impedimetric Detection of UVC-Induced DNA Damage

Neeraj Bangruwa, Manish Srivastava, and Debabrata Mishra*

Cite This: *ACS Omega* 2022, 7, 37705−37713

Read Online

ACCESS | Metrics & More | Article Recommendations | Supporting Information

ABSTRACT: In this work, we demonstrate chiral-induced spin selectivity (CISS)-based label-free electrochemical impedimetric detection of radiation-induced DNA damage using the electrons' spin as a novel tool of sensing. For this, self-assembled monolayers (SAMs) of short ds-DNA (of length 7.14 nm) are prepared on arrays of multilayer thin film devices comprising a gold overlay (500 μm diameter with 10 nm thickness) on a nickel thin film (100 nm) fabricated by the physical vapor deposition technique. Subsequently, the SAMs of ds-DNA are exposed to ultraviolet C (UVC) radiation for a prolonged period of 8 h to induce structural perturbations in DNA. The susceptibility of DNA to radiation-induced damage was probed by recording the spin-dependent electrochemical impedimetric spectra, wherein a continuous sinusoidal wave of the amplitude of 10 mV was superimposed on DC bias in the frequency range of 10^0−10^5 Hz, with simultaneous spin injection through the attached DNA. The inherent correlation between the charge-transfer resistance (R_{ct}) and the spin selectivity of electrons through DNA was taken into account for the detection of DNA damage for the first time with a limit of detection achieved up to 10 picomolar concentrations of DNA. As the spin-polarized electrons directly probe the structural symmetry, it is robust against perturbation from electronic signals usually found in conventional electrochemical biosensors.

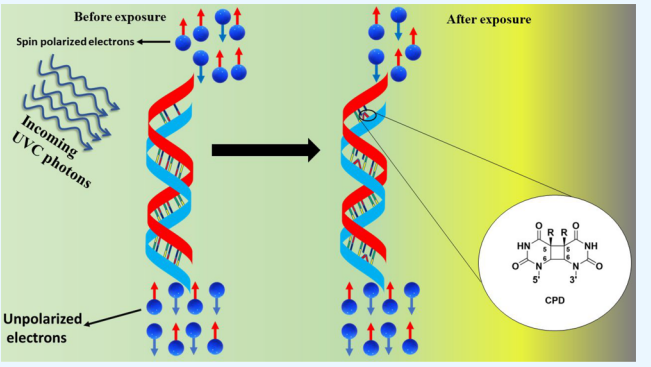

INTRODUCTION

Demonstration of the CISS effect using chiral molecules and its use in a variety of applications, including in enantioselection,[1,2] water splitting,[3,4] molecular spintronics,[5] and biorecognition,[6] is remarkable and is one of the most sought-after areas of research among academicians across the globe. The presence of structural asymmetry in the form of chirality in various biomolecules, such as DNA, proteins, and amino acids, leads to this observable effect when electrons pass through these molecules with a predefined quantization (of spin) axis. The outcome of the electrons' spin state in the form of spin polarization is precisely known as the CISS effect. For example, ds-DNA shows more than 60% of spin filtering at room temperature, while it lies in the range of 10−30% for most of the proteins and/or peptides.[7−9] The empirical manifestation of CISS effect through various kinds of devices prepared at the nanoscale and using nanojunction is ubiquitous. Excellent review articles have been published in recent years which shed light in detail about the applications and/or perspectives of the CISS effect.[10] In a significant contribution to the fundamental understanding of molecular interactions via charge reorganization, A. Kumar et al. observed experimentally that charge reorganization is accompanied by spin polarization for chiral molecules using a hall device and the same phenomenon could be used to prepare next. Similarly, in another experiment, R.A. Rosenberg et al. has shown experimentally that the spin-polarized electrons generated through DNA, due to CISS effect, interact differently with (R)- and (S)-epichlorohydrin enantiomers as estimated from the quantum yield of dissociation of those enantiomers.[11] From these observations, it is imperative that an ensemble of spin-polarized electrons, spontaneously generated by the CISS effect, can be used as the quantum mechanical tool for biorecognition/detection with enhanced sensitivity. One of the important areas of biomolecular detection is DNA damage detection which might occur due to its exposure to exogenous sources including ionizing radiation,[12,13] nonionizing radiation,[14] and chemicals.[15] Ultraviolet (UV) rays are one of the major electromagnetic radiations on earth's atmosphere and is a cause of concern for environmental pollution and/or hazards. Note that the spectra of UV radiation contain UVC rays, which fall in the range of 200−280 nm, comes from the sun, are readily absorbed by the ozone layer, and do not contribute to large-

Received: July 23, 2022
Accepted: October 6, 2022
Published: October 13, 2022

scale environmental pollution.[16] Nevertheless, other sources of UVC rays stem from man-made sources, such as arc welding torches, mercury lamps, UV sanitizing bulbs, etc., and pose a threat to human health.[17,18] UVC radiation, carrying the highest energy among its other variants (UVA and UVB), has the potential to damage the DNA and is a prime etiological factor in the formation of cytotoxic DNA lesions[19] including dimers and other photo products. UVC radiation damages DNA 10^6 times more than UVA radiation and 75% photoproducts/byproducts of it are the cyclobutane pyrimidine dimers (CPDs). Thus, it would be prudent to build an inexpensive, sensitive device to detect DNA damage caused by UVC radiation, which has gotten less attention than the higher wavelength-based UV radiations, such as UVA and UVB. Electrochemical impedance spectroscopy (EIS) is one of the important techniques for the detection of DNA damage. It is mainly based on integrated receptor-transducer devices that measure the electrical signal with DNA as the recognition element.[20−23] One of the major drawbacks of the conventional electrochemical techniques is that perturbation associated with the electronic signal/circuit might affect the output current/signal resulting in the spurious interpretation of data.[24,25] This can be avoided if the electronic charge current can be replaced with the spin-polarized current (CISS-induced) as the latter is not influenced by any external perturbation and solely depends on the intrinsic structural symmetry of the molecule for its manipulation. Any minute changes in the structure of DNA would affect the CISS phenomenon drastically.

Furthermore, the yield of spin-polarized electrons through a chiral molecule is highly sensitive to its secondary structure, such as length of the helix, pitch, etc., and provides structure-specific information. T. J. Zwang et al. have shown, by using the spin-dependent cyclic voltammetric technique, that the spin filtering by DNA strongly depends on its helix.[26] In a recently published work, we have demonstrated through spin-dependent cyclic voltammetry that there is a specific correlation between the electrons' spin and DNA structure using the CISS effect. It was observed that the yield of spin-polarized electrons through DNA decreases when the DNA is damaged by ionizing radiation, such as γ rays.[13] Nevertheless, it has been established both theoretically[27−30] and experimentally[8,31] that any kind of perturbation in the DNA structure, like DNA damage, base-pair mismatch, pitch,[29] and helix length,[8] affect the spin polarization through ds-DNA.

In this work, we have designed and developed a spin-based label-free impedimetric device for the first time to study UVC-induced DNA damage. We intend to study the effect of UVC radiation on the double strand (ds)-DNA by the spin-dependent EIS technique. For this, we have taken a thiol-modified 21-base pair DNA sequence (of 7.14 nm length size) with 53% GC content. We demonstrate that the yield of spin polarization through ds-DNA is commensurate with the structural changes made by UVC radiation in ds-DNA and can be quantitatively probed by a spin-dependent impedimetric DNA sensor. Our results rationalize the fact that spin can be used as a novel tool of detection for damaged DNA owing to the chirality present in the secondary structure of DNA.

2. EXPERIMENTAL SECTION

2.1. Materials. Twenty-one base long DNA primer and its reverse primer were procured from Sigma-Aldrich. All of the required chemicals, utilized in this work, were purchased from Sigma-Aldrich, including potassium hexacyanoferrate (III) [$K_3Fe(CN)_6$], potassium hexacyanoferrate (II) trihydrate [$K_4Fe(CN)_6{\cdot}3H_2O$], potassium chloride (KCl), and potassium phosphate (KH_2PO_4 and K_2HPO_4). Molecular grade water was purchased from G Biosciences, India. Granules of Cr, Ni, and Au (purity $\geq$ 99.99%) and silicon wafers N-type ⟨100⟩ (0.001−0.009 Ω-cm) of 480 ± 15 μm were purchased from Macwin India, India.

2.2. Fabrication of Ni/Au Thin-Film. The gold (Au) coated nickel (Ni) thin film devices were fabricated by the combined electron beam evaporation and thermal evaporation techniques at a high vacuum of 10^{-7} Torr base pressure. Ni thin film of thickness of 100 nm was evaporated over a chemically treated thermally oxidized silicon dioxide (SiO_2) surface with a 5 nm of chromium adhesion layer between Ni and SiO_2. Without breaking the vacuum, a shadow mask was used to make a patterned structure of Au nanolayer having a thickness of 10 nm over the Ni thin film with a diameter of 500 μm. The growth rate of deposition for all the materials was kept at 0.1 Å/s.

2.3. Preparation of Self-Assembled Monolayers of DNA. For the preparation of the self-assembled monolayers (SAMs) of DNA, ds-DNA was used on freshly prepared Ni/Au thin film. The sequence of the DNA employed in the present study is as follows: primer, DNA 5′-AACGTTGTCCGTCTC-CAGTTG-thiC3-3′, and reverse primer, 5′-CAACTGGA-GACGGACAACGTT-3′.

To assemble the monolayers of ds-DNA on Ni/Au, the thin film was boiled in 2-propanol and ethyl alcohol for 15 min each, then dried using nitrogen (N_2) gas. To remove traces of organic contaminants, present on the surface of the thin film, Ni/Au was exposed to UV light and quickly washed with ethyl alcohol, and again dried by N_2 jet. Subsequently, thiol modified DNA primer and its reverse primer of concentration of 10 μm were hybridized following a standard protocol in a clean environment.[32] Subsequently, the Ni/Au thin film was immersed in the solution of ds-DNA and was left for 24 h in dark for making SAMs of DNA. Note that −SH functional group makes the covalent bond with Au and helps in the formation of a monolayer. The thin film coated with SAMs of ds-DNA was gently washed with 0.1 M phosphate buffer saline (PBS) solution of pH 7.2 to discard unattached DNA and was dried with N_2 gas for further use.

2.4. Characterizations. Several techniques were used to characterize Ni/Au thin film after the fabrication of the electrodes and to confirm the formation of a monolayer. Scanning electron microscopy (SEM, JEOL Japan) was used for the morphological analysis of Ni/Au thin film while surface topography was studied by atomic force microscopy (AFM, PARK N X 10). The electrochemical workstation (CORRTEST CS350) was used for all the spin-dependent electrochemical measurements including electrochemical impedance spectroscopy (EIS). NICOLET iS50 Fourier transform-infrared (FT-IR) spectrophotometer was used to record the characteristic FT-IR spectra of SAM of DNA-coated Ni/Au thin film. X-ray diffraction (XRD) pattern of Ni/Au thin film was recorded by Rigaku Ultima IV X-ray diffractometer using Cu source of wavelength 1.54 nm. The monolayer of ds-DNA before and after UVC-irradiation was characterized by X-ray photoelectron spectroscopy (XPS, PHI 5000 Versa Probe III) with a photon energy of 280 eV.

https://doi.org/10.1021/acsomega.2c04659
ACS Omega 2022, 7, 37705−37713

3. RESULTS AND DISCUSSION

Various properties pertaining to morphological, topological, and spectroscopic behavior of bare Ni/Au thin film and/or molecular assembly of ds-DNA formed on the surface of the film have been characterized by using different techniques and the results are shown in Figure 1. Figure 1a shows the XRD

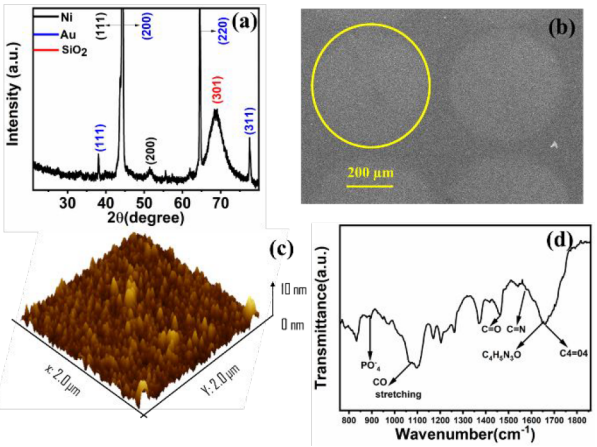

Figure 1. (a) XRD pattern, (b) SEM image of circular patches, (c) 3d-view of AFM image of Ni/Au thin film, and (d) FTIR spectrum of monolayers of ds-DNA immobilized on Ni/Au thin film.

pattern of as-prepared Ni/Au thin film. Diffraction peaks corresponding to the 2θ angles centered at 38.1°, 44.4°, 64.5°, and 77.5° match with (111), (200), (220), and (311) planes of Au overlayer.[33] Similarly, the peaks observed at 44.4° and 51.8° corresponds to the (111) and (200) planes underneath Ni metal;[34] the broad peak at 68.4° has been attributed to the (301) plane of SiO_2 substrates (JCPDS card no. 00-005-0490). These well-defined sharp peaks confirm the crystalline structure of Ni/Au thin film and are formed without any postheat treatment once the samples are made. The surface morphology of the as-prepared Ni/Au device was characterized by SEM and a representative image is shown in Figure 1b. The circular patches shown in Figure 1b are Au overlayer of the device with a diameter of 500 μm. The array of circular patches of Au constitutes a set of independent devices formed on the surface of Ni. The 3D view of the surface topography as simulated from the AFM image of the Au-overlayer is shown in Figure 1c. After the successful fabrication of Ni/Au devices, SAMs of DNA were immobilized on Ni/Au thin film by the procedure as described above using a standard protocol. The formation of SAMs of DNA was verified by recording the FT-IR spectra which confirms the presence of characteristic vibrational peaks of a different functional moiety of DNA molecule and are depicted in Figure 1d. Upon analyzing the spectroscopic data, it was found that the asymmetric and symmetric PO_4^- groups of the phosphodiester deoxyribose backbone specific to the distinctive peaks of ds-DNA in the region of 961−1260 $cm^{-1}$are present in the sample.[35] The peak observed at 1066 cm^{-1} is related to the symmetric CO stretching of the backbone. The peak at 1647 cm^{-1} corresponds to the cytosine while those obtained in the range of 1515−1650 cm^{-1} match with C═O, C═N, C═C stretching, and exocyclic $-NH_2$ bending vibrations in the DNA bases.[35−37] Similarly, the peak observed at 1660 cm^{-1} corresponds to the C4═O4 vibration in thymine.[36] The characteristic peaks of the different functional groups of DNA found in the FT-IR spectra confirm the assembly of the ds-DNA monolayer on Ni/Au thin film successfully.

Figure 2 represents the schematic illustration of the basic measurement setup and an array of Ni/Au devices prepared for

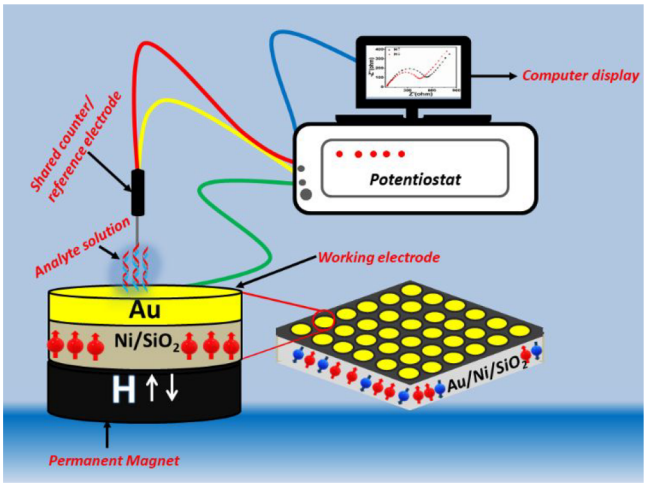

Figure 2. Schematic illustration of experimental setup: The two-electrode system consists of a SAM-coated Au/Ni thin film on a SiO_2 substrate, referred to as the working electrode (WE), and a platinum wire, acting as a pseudo-reference/counter electrode (CE), shown on the top of the liquid drop (left). Electrochemical measurements are done with an electrolyte (2 μL) containing 5 mM $K_4Fe(CN)_6/K_3Fe(CN)_6$ in phosphate buffer solution at pH 7.2 and a schematic view of the whole Ni/Au thin film device (right). The circular area represents an Au overlayer (10 nm) of diameter 500 μm on a continuous Ni surface. Note that the circular area is the active region that contains SAMs of DNA. A permanent Nd−Fe−B magnet of field strength 5000 Oe is placed below the device for magnetizing the Ni surface for spin injection. The experiment is done by a potentiostat and is recorded by a computer.

the measurement. The measurement was done in a two-electrode system using a potentiostat. The Ni/Au device and Pt wire were taken as working and pseudo-reference/counter electrodes, respectively. As shown in Figure 2, a small volume (2 μL) of the phosphate buffer solution containing redox couple (Fe^{3+}/Fe^{2+}) was cast gently on active circular patches containing SAMs of DNA. Note that the small drop of solution immerses SAMs of DNA and remains undisturbed on the Au overlayer and does not spread out due to the specially designed surrounding hydrophobic Ni surface. The counter electrode (Pt wire) was then gently placed from the top to make contact with the meniscus of the drop of analyte solution for completing the electrical circuit needed for measurement. To measure the spin selectivity by DNA molecule, a permanent magnet of field strength 5000 Oe was placed underneath the SiO_2 substrate containing Ni/Au device. Nickel was used in the present work to facilitate the spin injection through the self-assembled monolayer of DNA by a permanent magnet. A thin layer of Au overlayer was deposited on Ni, which is essential to form a covalent bond between the thiol group of DNA and Au, required for the molecular self-assembly. Note that the experiment is not limited to Ni only, but any ferromagnetic material which can be easily magnetized perpendicular to the surface of the thin film for spin injection can be used as an alternate material. Furthermore, we used Ni because it is more stable against corrosion than other ferromagnetic elements, such as Co or Fe. The thickness of Ni thin film used in the

https://doi.org/10.1021/acsomega.2c04659
ACS Omega 2022, 7, 37705−37713

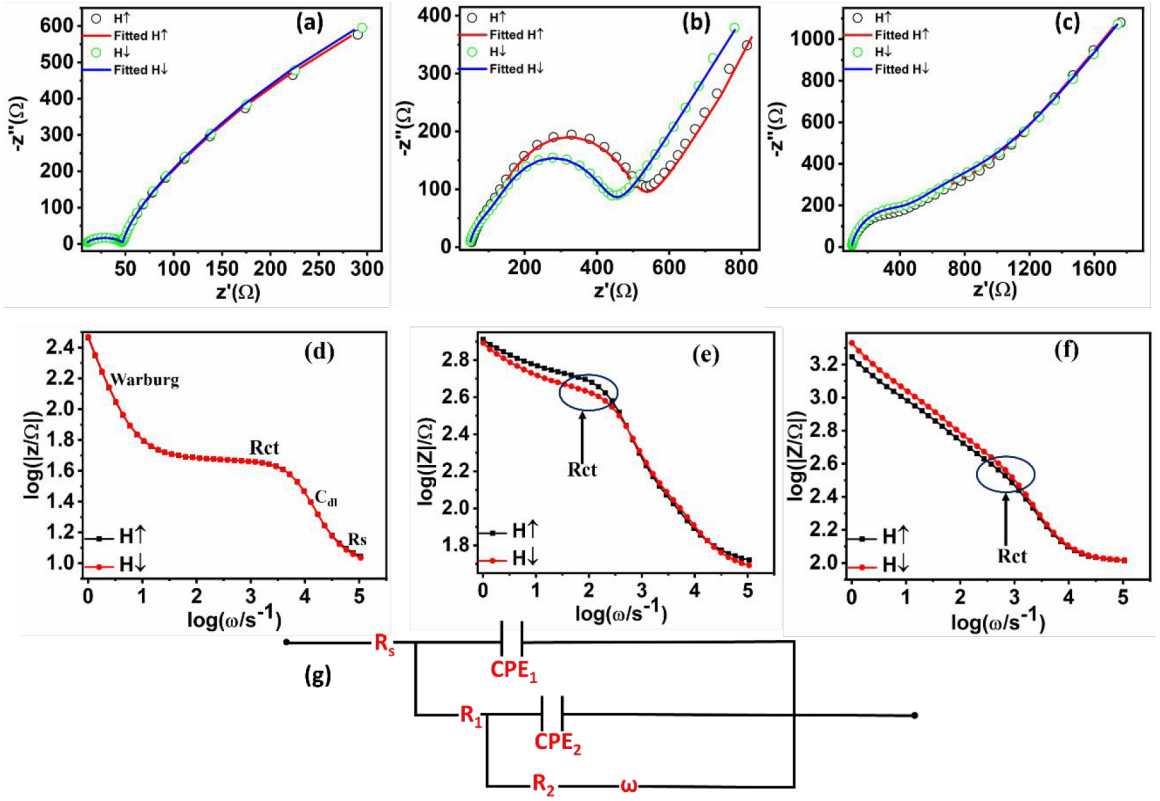

Figure 3. Nyquist plot (EIS) for (a) bare Ni/Au thin film, (b) SAMs of ds-DNA prior to UVC-irradiation, and (c) SAMs of ds-DNA after 8 h of UVC-irradiation immobilized on the Ni/Au thin film. The solid lines in panels a−c are the fitting of data points in Nyquist plot. Bode magnitude plot (EIS) for (d) bare Ni/Au thin film, (e) SAMs of ds-DNA before UVC-irradiation, (f) SAMs of ds-DNA after 8 h of UVC-irradiation immobilized on the Ni/Au thin film, and (g) Randles equivalent circuit diagram for Nyquist plot.

present study was varied and optimized at 100 nm for an efficient spin injection through the monolayers. A free-standing permanent magnet was placed vertically below the device in such a manner that the setup remained undisturbed during the process of measurement. The direction of the magnet was changed sequentially, either "UP" or "DOWN" to polarize the surface of Ni thin film with up spin and down spin, respectively. After applying the magnetic field normal to the surface of the sample, the electron with a particular spin orientation was injected through the monolayers by applying a bias voltage across the electrodes. The same process was repeated in the other direction of the magnetic field as well for the EIS measurements. Note that the quantization axis (Z) is normal to the surface of the film and is along the axis of the helix of DNA. SAM-coated Ni/Au thin film and Pt wire was used as working and reference/counter electrodes, respectively.[13,38] The redox couple $K_4[Fe(CN)_6]\cdot 3H_2O/K_3[Fe(CN)_6]$ with 5 mM concentration were used in the aqueous solution of PBS at pH 7.2.

Figure 3a−c shows the Nyquist plots of the EIS measurements of bare Ni/Au, DNA-coated Ni/Au thin film before and after exposure to UVC radiation. In this technique, a continuous potential wave of amplitude 10 mV was superimposed on DC bias in the frequency range of 10^0 Hz-10^5 Hz. To minimize the effect of electronic perturbation, open circuit potential (OCP) was used as DC bias. Note that, recording the value of R_{ct} (diameter of semicircle in EIS measurement) from Nyquist plot in SAM of DNA before and after exposure to UVC radiation would indicate the occurrence of damage/structural change in DNA and is the guiding principle behind traditional impedimetric DNA biosensors.[39,40] Nevertheless, in the present case, we estimated the difference in the value of R_{ct} (ΔR_{ct}) for both the directions of the applied magnetic field. The value of ΔR_{ct} calculated for the same DNA before and after the radiation exposure gave an estimate of structural change and is the underlying principle behind spin-dependent impedimetric biosensor used in the present work. Note that, any occurrence of finite ΔR_{ct} would indicate different charge transfer resistance for electrons with up and down spin configurations generated due to the CISS effect. Figure 3a depicts the EIS measurement of a bare Ni/Au device as a control experiment with $\Delta R_{ct} = 0$, and the corresponding spin polarization ($|P_S|$) value, calculated from ΔR_{ct} after fitting, was found to be 0% as expected. Figure 3b shows the result of SAMs of ds-DNA prior to UVC-irradiation on the surface of Ni/Au and exhibited a difference in the value of R_{ct} for spin (up and down) injection through ds-DNA. Subsequently, the $|P_S|$ was estimated for DNA and was found to be 10.38 ± 0.8% before radiation exposure. Figure 3c represents the Nyquist plot for the ds-DNA after 8 h of exposure to UVC radiation with a constant radiation flux (≈250 kJ m^{-2} h^{-1}) and $|P_S|$ was found to be 0.91 ± 0.8%. The EIS spectra have been fitted with the Randles equivalent circuit and are shown in Figure 3g. Various parameters extracted from the fitting of the data are summarized in Table S1. The apparent decrease in the value of $|P_S|$ can be attributed to the breaking of hydrogen bonds in ds-DNA and/or to the formation of cyclobutane pyrimidine dimers including other photoproducts such as pyrimidine (6−4) pyrimidone photoproduct ((6−4) PP) as per the study available in the literature.[41−43] The formation of CPDs is due

https://doi.org/10.1021/acsomega.2c04659
ACS Omega 2022, 7, 37705−37713

to the formation of bonding between the neighboring thymine bases. Note that CPDs introduce conformational changes in DNA, which perturbs the structural symmetry in the secondary structure(helix) of DNA and leads to the formation of kinks in the double helix structure. This eventually impedes the spin-polarized electrons transferred through DNA resulting in a low value of $|P_S|$ that has been found experimentally in the present study as mentioned above. We also performed the spin-dependent cyclic voltammetric measurements on these samples and the results are in accordance with that of EIS measurements (see Figure S1).

The EIS measurements can also be interpreted as in the Bode magnitude plot. Figure 3d−e depicts the Bode magnitude plot, in which log of the magnitude of the impedance ($|Z|$) vs the log of frequency (ω) is plotted. Several parameters can be extracted from the Bode magnitude plot, including ω, R_{ct}, C_{dl}, and R_s.[44]Figure 3d−e depicts the Bode magnitude plot for bare device and SAM of ds-DNA on Ni/Au device before and after the UVC-irradiation, respectively. An appreciable deviation in the curvature of graphs obtained for two different directions of applied magnetic field for ds-DNA indicate the CISS effect, which is shown in Figure 3e. However, it is absent in bare Ni/Au devices for obvious reasons already mentioned in the preceding section (see Figure 3d). Nevertheless, a negligible effect of CISS was observed for the same ds-DNA after it was exposed to UVC for a prolonged period shown in Figure 3f. These results are in accordance with that of the Nyquist plot for the confirmation of structure-specific spin-polarized electron transfer through DNA. The impedimetric measurements were done on different concentrations of DNA samples taken to make the monolayer. In order to find out the limit of detection for the spin-based device, various concentrations of DNA molecules were prepared and the same procedure was followed for all the cases. We could achieve DNA damage detection up to 10 picomolar concentrations of DNA and the response time of the electrochemical device was found to be 8 min which is defined as the time required to perform one measurement to estimate the value of $|P_S|$. This shows the applicability of the prepared impedimetric sensors at low concentration. Apart from the limit of detection, the practical application of impedimetric biosensor depends on its robustness and reproducibility.

To examine the reproducibility of the impedimetric UVC biosensor, three arrays of devices were tested independently to detect the damaged DNA multiple times using these devices. The relative R_{ct} (rR_{ct})with the number of electrodes for the magnetic field up (Figure 4a) and down direction (Figure 4b) is presented. The sensor response is represented by rR_{ct}, which is the relative R_{ct} difference between SAMs of ds-DNA and the bare Au/Ni thin film.[45] The corresponding mathematical expression used can be expressed as

$$rR_{ct} = \frac{R_{ctDNA} - R_{ctNi/Au}}{R_{ctNi/Au}}$$

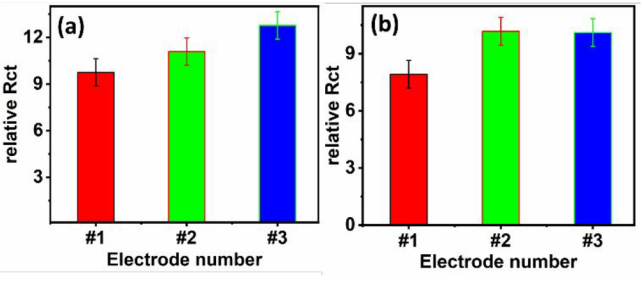

Figure 4. Reproducibility assessment of the UVC-damaged impedimetric sensor for (a) spin up and (b) spin down direction of injected electrons through SAMs of ds-DNA.

The standard error of mean was calculated for all the devices and was found to be 0.88 and 0.73 for the Figure 4a and b, respectively.

Recently, S. Mishra et al. has proved experimentally that oxidatively damaged DNA either increases or decreases the yield of CISS-generated spin-polarized electrons.[29] They have proved experimentally that the enhanced or reduced spin filtering effect of damaged DNA is dependent on the trajectory of electrons' path through DNA. However, in the present case, we found a diminished spin filtering effect in UVC-induced damaged DNA. Note that DNA molecule is susceptible to absorbing UVC radiation and cause many cytotoxic and mutagenic DNA lesions including single and/or double-strand breaks (SSBs, DSBs) in the DNA helix. The most common pyrimidine dimers formed after the UVC exposure to ds-DNA are the cyclobutene pyrimidine dimers (also known as thymine dimers), followed by (6−4) pyrimidine photoproduct (6−4 PPs). Figure 5a depicts the possible effect of UVC radiation on ds-DNA and their structure. When UVC is irradiated onto ds-DNA, hydrogen bonds between the thymine and adenine begin to break, and a cyclobutane ring is formed as a result of the formation of a double covalent bond between C5−C5 and C6−C6 atoms of each thymine−thymine (T<>T) base, and 6−4 PPs formed as a result of a single covalent bond between C4−C6 atoms. Figure 5b represents the schematic illustration of the radiation-induced effect in ds-DNA.

To verify the conformational change taking place in ds-DNA subject to UVC exposure and its implications on spin filtering percentage, XPS spectra were recorded. Figure 6 depicts the XPS survey scans of SAMs of ds-DNA on Ni/Au thin film before and after UVC irradiation after 0 and 8 h. XPS spectra of SAMs of DNA show the elemental composition of the molecule containing C 1s, N 1s, P 2p, and O 1s corresponding to their binding energies (BEs).[46−48] The presence of some extra elements, including sulfur and gold in XPS spectra confirms the assembly of ds-DNA on Au over layer.[46]

The atomic percentage extracted from the spectra after exposing the UVC radiation for t = 0 and 8 h are summarized in Table 1. It shows a decrease in the atomic percent of elements after exposure to UVC. The deconvoluted peaks of all the constituent elements of DNA are given in Supporting Information (see Figures S2 and S3) and corresponding Table S2.

To further supplement the XPS results, possible formation of by products in the secondary structure of DNA was investigated by FT-IR. Figure 7 depicts the UV absorption spectra and FT-IR spectra of SAMs of ds-DNA prior to and after exposure to UVC radiation and difference spectra. We observed a clear shift in the peak position of all characteristic peaks of different functional groups of DNA. For example, the peak at 1660 and 894 cm^{-1} shifted to 1670 and 896 cm^{-1} respectively (Figure 7a).[49] These results confirm that the change in the conformation of DNA occurs after the radiation exposure, which has a specific effect on the spin filtering ability of ds-DNA. The difference spectra were obtained by subtracting the FT-IR spectrum of unexposed DNA from

https://doi.org/10.1021/acsomega.2c04659
ACS Omega 2022, 7, 37705−37713

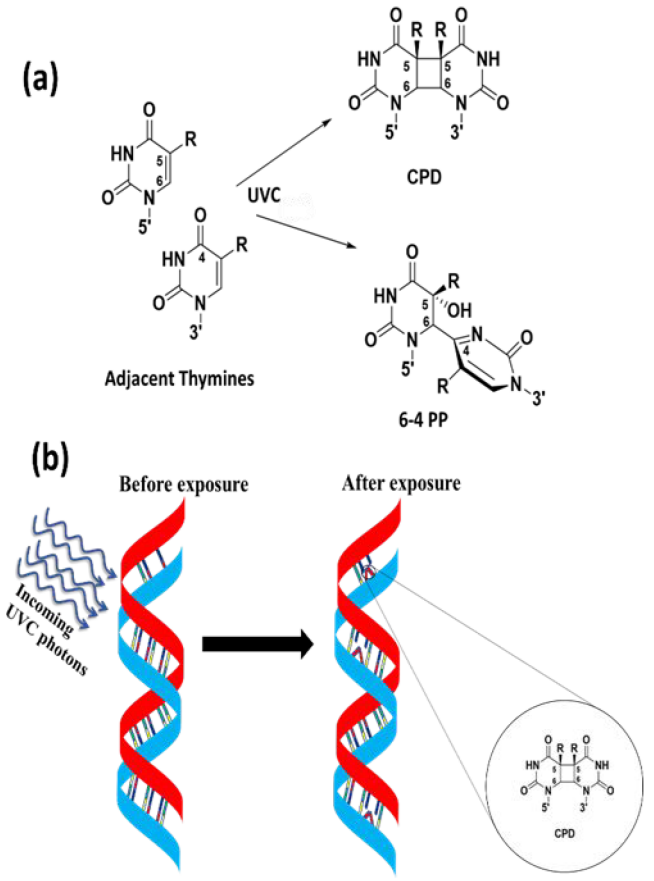

Figure 5. (a) Structure of cyclobutane pyrimidine dimer and (6−4) pyrimidine photoproduct after UVC irradiation to DNA and structure of 5′−3′ thymines in DNA. (b) Schematic illustration of ds-DNA prior to and after the exposure to UVC radiation and the magnified view of the formation of single CPD. Bases arranged in the schematic view of ds-DNA are according to the sequences taken in this measurement. Yellow = guanine, green = cytosine, red = thymine, and blue = adenine.

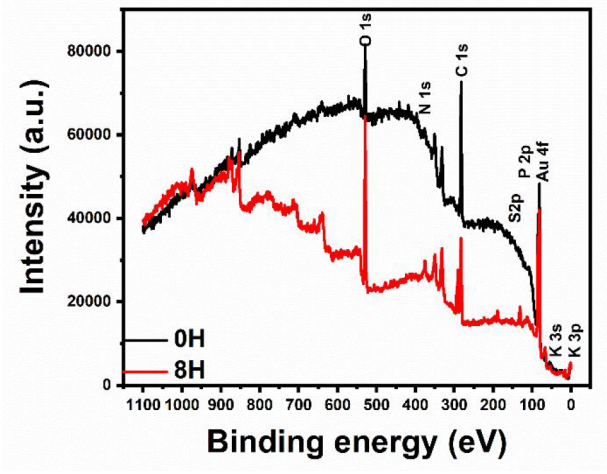

Figure 6. A survey XPS spectrum of monolayers of ds-DNA on an Ni/Au thin film before (black) and after 8 h of UVC-irradiation (red).

that of UVC-exposed ds-DNA to detect FT-IR marker bands that are indicative of dimerization (Figure 7b). After the exposure of ds-DNA to UVC radiation, two major pyrimidine photoproducts are formed in the ds-DNA, such as CPDs and

Table 1. Elemental Composition in ds-DNA Monolayers and Their Atomic Percentage as Extracted from the XPS Spectra at 0 and 8 h of UVC-Irradiation

sl. no.	atoms	atomic percentage before UVC irradiation	atomic percentage after UVC irradiation
1	C 1s	74.8	70.9
2	N 1s	2.7	0.5
3	O 1s	10.4	21.8
4	P 2p	9.3	6.0
5	S 2p	2.8	0.9
6	Au 4f	<0.1	<0.1

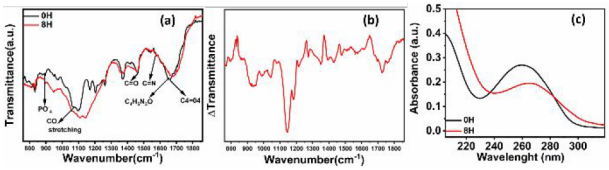

Figure 7. (a) FT-IR spectra of the SAMs of ds-DNA for the exposure time for 0 and 8 h. (b) Difference spectra obtained by subtracting the FT-IR spectrum from each spectrum of UVC irradiated ds-DNA and (c) UV absorption spectra of the SAMs of ds-DNA for the exposure time of 0 and 8 h. Color codes are same for panels a−c.

6−4PPs.[37,49,50] However, 6−4 PPs can be neglected because of very low yields in comparison to CPDs. Furthermore, UVC-exposed ds-DNA immobilized on Ni/Au thin film resulted in the emergence of numerous positive and negative differences in bands, which may be ascribed to the formation of thymine dimers. The positive peaks at 1464 and 1403 cm^{-1} and the negative peak at 1425 cm^{-1} correspond to the CPDs. Thus, it can be concluded that the formation of complexes in ds-DNA due to UVC exposure has resulted in the retarded spin selectivity of DNA. It can be concluded that spin-based impedimetric devices for DNA damage detection is a novel way to sense the structural changes occurring in ds-DNA due to UVC radiation.

UV absorption spectra are also used to detect the damage in ds-DNA and the formation of CPDs in ds-DNA. Figure 7c depicts the UV absorption spectra of SAMs of ds-DNA before and after the exposure to UVC radiation. The absorption peak of ds-DNA at 260 nm was observed before the UVC irradiation and after the UVC irradiation for 8 h the absorption peak at 260 nm has been found to decrease, representing the UVC radiation-induced DNA damage by disrupting the π-conjugation.[43] In contrast, adenine and guanine could not undergo UVC-induced damage.

The comparison between electronic current and spin current-based electrochemistry is described in Table 2.

4. CONCLUSIONS

In summary, a novel spin-based electrochemical impedimetric biosensor was rationally designed and developed for the detection of UVC-induced DNA damage for the first time. Spin-polarized electrons generated due to CISS effect were used to quantitatively access the structural damage in DNA. For this, SAMs of DNA were prepared on Ni/Au device and impedimetric measurements were done with spin injection in the frequency range of 10^0−10^5 Hz. We observed that the charge transfer resistance R_{ct} was related intrinsically to the absolute spin polarization value $|P_S|$. DNA damage was associated with a significant decrease in $|P_S|$ value that was

https://doi.org/10.1021/acsomega.2c04659
ACS Omega 2022, 7, 37705−37713

Table 2. Comparative Table for Traditional and CISS-Based Electrochemical Techniques for the Detection of Damaged DNA

traditional electrochemistry for DNA damage detection	CISS-based electrochemistry for DNA damage detection
1. Measures the value of absolute current (I) for the detection of DNA damage.	1. Measures the spin-polarized current (ΔI) for the detection of DNA damage.
2. Measured current (I) is silent on the structure of DNA.	2. Extracted current (ΔI) probes the possible changes in the structure of DNA.
3. Possibility of artifact in the measured current/signal.	3. No role of artifact in the measured spin-polarized current (ΔI).
4. Charge-transfer resistance (R_{ct}) in the Nyquist plot either increases or decreases for damaged DNA as reported.[43,51,52]	4. The difference in the value of charge transfer resistance (ΔR_{ct}) always decreases for damaged DNA.
5. Few labels may be required for the detection of DNA damage which makes it costly.	5. It is completely label-free and also a cost-effective technique.

found to be 0.91 ± 0.8%. The apparent decrease in $|P_S|$ value has been attributed to the formation of CPDs in the helix of DNA and the formation of the same was verified experimentally by using several techniques including XPS, UV spectroscopy and FTIR. The impeding spin filtering effect of DNA is due to the alteration of structural symmetry needed to generate spin-polarized electrons. We believe, our results would inspire researchers and scientists around the globe to make efficient spin-based DNA sensors.

■ ASSOCIATED CONTENT

Data Availability Statement

The data that support the findings of this study are available from the corresponding author upon reasonable request.

Supporting Information

The Supporting Information is available free of charge at https://pubs.acs.org/doi/10.1021/acsomega.2c04659.

EIS results supported by the spin-dependent cyclic voltammetry; parameters extracted from the Nyquist plot using the Randles equivalent circuit; and confirmation of SAMs of DNA by XPS spectra (PDF)

■ AUTHOR INFORMATION

Corresponding Author

Debabrata Mishra − *Department of Physics and Astrophysics, University of Delhi, New Delhi 110007, India;* orcid.org/0000-0001-9685-1886; Email: dmishra@physics.du.ac.in

Authors

Neeraj Bangruwa − *Department of Physics and Astrophysics, University of Delhi, New Delhi 110007, India;* orcid.org/0000-0002-7101-0359

Manish Srivastava − *Department of Chemical Engineering and Technology, Indian Institute of Technology, (BHU), Varanasi 221005, India;* orcid.org/0000-0002-0957-1251

Complete contact information is available at: https://pubs.acs.org/10.1021/acsomega.2c04659

Author Contributions

N.B: Data Curation, Analysis, and Manuscript writing; M.S.: Analysis, Manuscript writing; D.M.: Conceptualization, Analysis, Manuscript writing.

Notes

The authors declare no competing financial interest.

■ ACKNOWLEDGMENTS

D.M. acknowledges the financial support from MHRD-DST through Grant No. IMP/2018/001668, partial support from SERB through grant number CRG/2018/004264 and IoE, University of Delhi through Grant No. /IoE/2021/12/FRP from UGC through Grant No. F.4-5 (202-FRP)/2015 (BSR). N.B. is thankful to UGC-New Delhi for providing financial support. M.S. acknowledges the Science and Engineering Research Board for SERB Research Scientist award [SB/SRS/2018-19/48/PS] and also DST for DST INSPIRE Faculty award [IFA-13-MS-02].

■ REFERENCES

(1) Tassinari, F.; Amsallem, D.; Bloom, B. P.; Lu, Y.; Bedi, A.; Waldeck, D. H.; Gidron, O.; Naaman, R. Spin-Dependent Enantioselective Electropolymerization. *J. Phys. Chem. C* **2020**, *124* (38), 20974−20980.

(2) Metzger, T. S.; Siam, R.; Kolodny, Y.; Goren, N.; Sukenik, N.; Yochelis, S.; Abu-Reziq, R.; Avnir, D.; Paltiel, Y. Dynamic Spin-Controlled Enantioselective Catalytic Chiral Reactions. *J. Phys. Chem. Lett.* **2021**, *12* (23), 5469−5472.

(3) Zhang, W.; Banerjee-Ghosh, K.; Tassinari, F.; Naaman, R. Enhanced electrochemical water splitting with chiral molecule-coated Fe3O4 nanoparticles. *ACS Energy Lett.* **2018**, *3* (10), 2308−2313.

(4) Bhartiya, P. K.; Srivastava, M.; Mishra, D. Chiral-induced enhanced electrocatalytic behaviour of cysteine coated bifunctional Au−Ni bilayer thin film device for water splitting application. *Int. J. Hydrog. Energy* **2021**, DOI: 10.1016/j.ijhydene.2021.08.219.

(5) Mondal, P. C.; Mtangi, W.; Fontanesi, C. Chiro-Spintronics: Spin-Dependent Electrochemistry and Water Splitting Using Chiral Molecular Films. *Small methods.* **2018**, *2* (4), 1700313.

(6) Kumar, A.; Capua, E.; Kesharwani, M. K.; Martin, J. M.; Sitbon, E.; Waldeck, D. H.; Naaman, R. Chirality-induced spin polarization places symmetry constraints on biomolecular interactions. *PNAS.* **2017**, *114* (10), 2474−2478.

(7) Göhler, B.; Hamelbeck, V.; Markus, T.; Kettner, M.; Hanne, G.; Vager, Z.; Naaman, R.; Zacharias, H. Spin selectivity in electron transmission through self-assembled monolayers of double-stranded DNA. *Science.* **2011**, *331* (6019), 894−897.

(8) Mishra, S.; Mondal, A. K.; Pal, S.; Das, T. K.; Smolinsky, E. Z.; Siligardi, G.; Naaman, R. Length-dependent electron spin polarization in oligopeptides and DNA. *J. Phys. Chem. C* **2020**, *124* (19), 10776−10782.

(9) Mishra, D.; Markus, T. Z.; Naaman, R.; Kettner, M.; Göhler, B.; Zacharias, H.; Friedman, N.; Sheves, M.; Fontanesi, C. Spin-dependent electron transmission through bacteriorhodopsin embedded in purple membrane. *PNAS.* **2013**, *110* (37), 14872−14876.

(10) Aiello, C. D.; Abendroth, J. M.; Abbas, M.; Afanasev, A.; Agarwal, S.; Banerjee, A. S.; Beratan, D. N.; Belling, J. N.; Berche, B.; Botana, A.; et al. A Chirality-Based Quantum Leap. *ACS Nano* **2022**, *16* (4), 4989−5035.

(11) Rosenberg, R. A.; Mishra, D.; Naaman, R. Chiral Selective Chemistry Induced by Natural Selection of Spin-Polarized Electrons. *Angew. Chem., Int. Ed.* **2015**, *127* (25), 7403−7406.

(12) Mavragani, I. V.; Nikitaki, Z.; Kalospyros, S. A.; Georgakilas, A. G. Ionizing radiation and complex DNA damage: from prediction to detection challenges and biological significance. *Cancers.* **2019**, *11* (11), 1789.

(13) Bangruwa, N.; Srivastava, M.; Mishra, D. Radiation-Induced Effect on Spin-Selective Electron Transfer through Self-Assembled Monolayers of ds-DNA. *Magnetochemistry.* **2021**, *7* (7), 98.

(14) Gupta, S.; Sharma, R. S.; Singh, R. Non-ionizing radiation as possible carcinogen. *Int. J. Environ. Health Res.* **2022**, *32* (4), 916−940.
(15) Poirier, M. C.The Role of DNA Damage in Cancers Caused by Chemicals. In *Carcinogens, DNA Damage and Cancer Risk: Mechanisms of Chemical Carcinogenesis*; World Scientific, 2019; pp 1−19. DOI: 10.1142/9789813237209_0001.
(16) Krupa, S. V.; Kickert, R. N. The greenhouse effect: impacts of ultraviolet-B (UV-B) radiation, carbon dioxide (CO2), and ozone (O3) on vegetation. *Environ. Pollut.* **1989**, *61* (4), 263−393.
(17) Silva, L. G.; Moreira, F. C.; Souza, A. A.; Souza, S. M.; Boaventura, R. A.; Vilar, V. J. Chemical and electrochemical advanced oxidation processes as a polishing step for textile wastewater treatment: A study regarding the discharge into the environment and the reuse in the textile industry. *J. Clean. Prod.* **2018**, *198*, 430−442.
(18) López, M.; Palou, E.; Barbosa, C.; Tapia, M.; Cano, M. Ultraviolet light and food preservation. *Novel Food Processing Technologies* **2005**, 405−421.
(19) Bischof, K.; Hanelt, D.; Wiencke, C.UV radiation and Arctic marine macroalgae. In *UV Radiation and Arctic Ecosystems*; Springer, 2002; pp 227−243. DOI: 10.1007/978-3-642-56075-0_11.
(20) Liu, M.; Xu, J.; Yang, F.; Gu, Y.; Chen, H.; Wang, Y.; Li, F. Sensitive electrochemical detection of DNA damage based on in situ double strand growth via hybridization chain reaction. *Anal Bioanal Chem.* **2017**, *409* (29), 6821−6829.
(21) Mousavisani, S. Z.; Raoof, J. B.; Ojani, R.; Bagheryan, Z. An impedimetric biosensor for DNA damage detection and study of the protective effect of deferoxamine against DNA damage. *Bioelectrochemistry.* **2018**, *122*, 142−148.
(22) Zangeneh, M. M.; Norouzi, H.; Mahmoudi, M.; Goicoechea, H. C.; Jalalvand, A. R. Fabrication of a novel impedimetric biosensor for label free detection of DNA damage induced by doxorubicin. *Int. J. Biol. Macromol.* **2019**, *124*, 963−971.
(23) Ziyatdinova, G.; Labuda, J. Complex electrochemical and impedimetric evaluation of DNA damage by using DNA biosensor based on a carbon screen-printed electrode. *Anal. Methods.* **2011**, *3* (12), 2777−2782.
(24) Lv, S.; Zhang, K.; Zhu, L.; Tang, D.; Niessner, R.; Knopp, D. H2-based electrochemical biosensor with Pd nanowires@ ZIF-67 molecular sieve bilayered sensing interface for immunoassay. *Anal. Chem.* **2019**, *91* (18), 12055−12062.
(25) Gao, Y.; Zeng, Y.; Liu, X.; Tang, D. Liposome-mediated in situ formation of Type-I heterojunction for amplified photoelectrochemical immunoassay. *Anal. Chem.* **2022**, *94* (11), 4859−4865.
(26) Zwang, T. J.; Hurlimann, S.; Hill, M. G.; Barton, J. K. Helix-dependent spin filtering through the DNA duplex. *J. Am. Chem. Soc.* **2016**, *138* (48), 15551−15554.
(27) Eremko, A.; Loktev, V. Spin sensitive electron transmission through helical potentials. *Phys. Rev. B* **2013**, *88* (16), 165409.
(28) Geyer, M.; Gutierrez, R.; Cuniberti, G. Effective Hamiltonian model for helically constrained quantum systems within adiabatic perturbation theory: Application to the chirality-induced spin selectivity (CISS) effect. *J. Chem. Phys.* **2020**, *152* (21), 214105.
(29) Guo, A.-M.; Sun, Q.-f. Spin-selective transport of electrons in DNA double helix. *Phys. Rev. Lett.* **2012**, *108* (21), 218102.
(30) Gutierrez, R.; Díaz, E.; Naaman, R.; Cuniberti, G. Spin-selective transport through helical molecular systems. *Phys. Rev. B* **2012**, *85* (8), 081404.
(31) Mishra, S.; Poonia, V. S.; Fontanesi, C.; Naaman, R.; Fleming, A. M.; Burrows, C. J. Effect of oxidative damage on charge and spin transport in DNA. *J. Am. Chem. Soc.* **2019**, *141* (1), 123−126.
(32) Kumar, K. S.; Naaman, R. Quantitative analysis and characterization of self-assembled DNA on a silver surface. *Langmuir.* **2012**, *28* (41), 14514−14517.
(33) Dutta, I.; Munns, C.; Dutta, G. An X-ray diffraction (XRD) study of vapor deposited gold thin films on aluminum nitride (A1N) substrates. *Thin Solid Films.* **1997**, *304* (1−2), 229−238.
(34) Pilban Jahromi, S.; Huang, N. M.; Kamalianfar, A.; Lim, H. N.; Muhamad, M. R.; Yousefi, R. Facile synthesis of porous-structured nickel oxide thin film by pulsed laser deposition. *J. Nanomater.* **2012**, *2012*, No. 173825.
(35) Patel, M. K.; Solanki, P. R.; Kumar, A.; Khare, S.; Gupta, S.; Malhotra, B. D. Electrochemical DNA sensor for Neisseria meningitidis detection. *Biosens. Bioelectron.* **2010**, *25* (12), 2586−2591.
(36) Banyay, M.; Sarkar, M.; Gräslund, A. A library of IR bands of nucleic acids in solution. *Biophys. Chem.* **2003**, *104* (2), 477−488.
(37) Muntean, C. M.; Dina, N. E.; Tăbăran, A.; Gherman, A. M.; Fălămaş, A.; Olar, L. E.; Colobăţiu, L. M.; Ştefan, R. Identification of Salmonella serovars before and after ultraviolet light irradiation by Fourier transform infrared (FT-IR) spectroscopy and chemometrics. *Anal. Lett.* **2021**, *54* (1−2), 150−172.
(38) Faure, M.; Pallandre, A.; Chebil, S.; Le Potier, I.; Taverna, M.; Tribollet, B.; Deslouis, C.; Haghiri-Gosnet, A.-M.; Gamby, J. Improved electrochemical detection of a transthyretin synthetic peptide in the nanomolar range with a two-electrode system integrated in a glass/PDMS microchip. *Lab Chip.* **2014**, *14* (15), 2800−2805.
(39) Qiu, Z.; Tang, D.; Shu, J.; Chen, G.; Tang, D. Enzyme-triggered formation of enzyme-tyramine concatamers on nanogold-functionalized dendrimer for impedimetric detection of Hg (II) with sensitivity enhancement. *Biosens. Bioelectron.* **2016**, *75*, 108−115.
(40) Xu, M.; Gao, Z.; Wei, Q.; Chen, G.; Tang, D. Hemin/G-quadruplex-based DNAzyme concatamers for in situ amplified impedimetric sensing of copper (II) ion coupling with DNAzyme-catalyzed precipitation strategy. *Biosens. Bioelectron.* **2015**, *74*, 1−7.
(41) Madsen, M. M.; Jones, N. C.; Nielsen, S. B.; Hoffmann, S. V. On the wavelength dependence of UV induced thymine photolesions: a synchrotron radiation circular dichroism study. *Phys. Chem. Chem. Phys.* **2016**, *18* (44), 30436−30443.
(42) Sproul, C. D.; Mitchell, D. L.; Rao, S.; Ibrahim, J. G.; Kaufmann, W. K.; Cordeiro-Stone, M. Cyclobutane pyrimidine dimer density as a predictive biomarker of the biological effects of ultraviolet radiation in normal human fibroblast. *Photochem. Photobiol.* **2014**, *90* (1), 145−154.
(43) Huo, H.; He, Y.; Chen, W.; Wu, L.; Yi, X.; Wang, J. Simultaneously monitoring UVC-induced DNA damage and photoenzymatic repair of cyclobutane pyrimidine dimers by electrochemical impedance spectroscopy. *Talanta.* **2022**, *239*, 123081.
(44) Dhillon, S.; Kant, R. J. Theory for electrochemical impedance spectroscopy of heterogeneous electrode with distributed capacitance and charge transfer resistance. *J. Chem. Sci.* **2017**, *129* (8), 1277−1292.
(45) Lin, L. P.; Tham, S.-Y.; Loh, H.-S.; Tan, M. T. Biocompatible graphene-zirconia nanocomposite as a cyto-safe immunosensor for the rapid detection of carcinoembryonic antigen. *Sci. Rep.* **2021**, *11* (1), 1−17.
(46) Lee, C.-Y.; Gong, P.; Harbers, G. M.; Grainger, D. W.; Castner, D. G.; Gamble, L. J. Surface coverage and structure of mixed DNA/alkylthiol monolayers on gold: characterization by XPS, NEXAFS, and fluorescence intensity measurements. *Anal. Chem.* **2006**, *78* (10), 3316−3325.
(47) Rosenberg, R.; Symonds, J.; Vijayalakshmi, K.; Mishra, D.; Orlando, T.; Naaman, R. The relationship between interfacial bonding and radiation damage in adsorbed DNA. *Phys. Chem. Chem. Phys.* **2014**, *16* (29), 15319−15325.
(48) Gomes, P.; Ferraria, A.; Botelho do Rego, A.; Hoffmann, S.; Ribeiro, P.; Raposo, M. Energy thresholds of DNA damage induced by UV radiation: An XPS study. *J. Phys. Chem. B* **2015**, *119* (17), 5404−5411.
(49) Schreier, W. J.; Schrader, T. E.; Koller, F. O.; Gilch, P.; Crespo-Hernández, C. E.; Swaminathan, V. N.; Carell, T.; Zinth, W.; Kohler, B. Thymine dimerization in DNA is an ultrafast photoreaction. *Science.* **2007**, *315* (5812), 625−629.
(50) Schleicher, E.; Heßling, B.; Illarionova, V.; Bacher, A.; Weber, S.; Richter, G.; Gerwert, K. Light-induced reactions of Escherichia coli

DNA photolyase monitored by Fourier transform infrared spectroscopy. *FEBS J.* **2005**, *272* (8), 1855−1866.
(51) Mousavisani, S. Z.; Raoof, J.-B.; Cheung, K. Y.; Camargo, A. R. H.; Ruzgas, T.; Turner, A. P.; Mak, W. C. Integrating an ex-vivo skin biointerface with electrochemical DNA biosensor for direct measurement of the protective effect of UV blocking agents. *Biosens. Bioelectron.* **2019**, *128*, 159−165.
(52) Svitková, V.; Nemčeková, K.; Vyskočil, V. Application of silver solid amalgam electrodes in electrochemical detection of DNA damage. *Anal. Bioanal. Chem.* **2022**, 5435−5444.

https://doi.org/10.1021/acsomega.2c04659
ACS Omega 2022, 7, 37705−37713